

Structural and morphological investigations on DC-magnetron-sputtered nickel films deposited on Si (100)

B. Geetha Priyadarshini · S. Aich · M. Chakraborty

Received: 13 August 2010 / Accepted: 6 December 2010 / Published online: 16 December 2010
© Springer Science+Business Media, LLC 2010

Abstract Pure nickel thin films were deposited on Si (100) substrates under different conditions of sputtering using direct current magnetron sputtering from a nickel metal target. The different deposition parameters employed for this study are target power, argon gas pressure, substrate temperature and substrate-bias voltage. The films exhibited high density of void boundaries with reduction in $\langle 111 \rangle$ texture deposited under high argon gas pressures. At argon gas pressure of 5 mTorr and target power of 300 W, Ni deposition rate was ~ 40 nm/min. In addition, coalescence of grains accompanied with increase in the film texture was observed at high DC power. Ni films undergo morphological transition from continuous, dense void boundaries to microstructure free from voids as the substrate-bias voltage was increased from -10 to -90 V. Furthermore, as the substrate temperature was increased, the films revealed strong $\langle 111 \rangle$ fiber texture accompanied with near-equiaxed grain structure. Ni films deposited at 770 K showed the layer-by-layer film formation which lead to dense, continuous microstructure with increase in the grain size.

Introduction

Nickel thin film deposited on different substrates by physical vapor deposition (PVD), chemical vapor deposition (CVD),

electroplating, and electroless deposition process exhibit varied mechanical, electrical, chemical or magnetic properties. Fabrication of nickel-based thin film materials is a subject matter of scientific interest due to their broad array of application ranging from contact devices to Li storage materials [1–6]. Magnetic-nickel thin films grown on substrates like SiO_2/Si , GaAs, MgO has opened up opportunities for various technological applications [7–10]. Particularly nickel films deposited using PVD technique possess good corrosion and wear resistant on steel substrates [10]. In addition, nanocrystalline nickel films deposited on Si substrates serves as infrared reflecting layer in black chrome solar selective surface and acts as a solar absorbing material [11]. Extensive studies on Ni/Si system were carried out for past few decades which primarily focused on the development of ohmic contacts and local interconnectors in CMOS devices owing to low resistivity and stress of nickel silicide [12–16]. On the other hand, nickel thin film deposition has also extended its attention towards the fabrication of Ni–Ti based shape memory alloy thin films for microactuator applications. As reported in the literature, there are various routes to fabricate Ni–Ti based alloy thin film by sputter-deposition technique. These include deposition either by sputtering from Ni–Ti alloy targets [17–22], alternate multilayer deposition of Ni and Ti [23–25] or by co-sputtering from elemental Ni and Ti targets on silicon substrates [26–29]. However, one of the prime requisites for realization of shape memory behavior in Ni–Ti alloy thin film is the near-equiatom composition of Ni and Ti. Co-deposition from elemental Ni and Ti targets is considered to be the most feasible technique to fulfill the purpose, since individual composition can be easily controlled during the deposition by varying individual target power [26]. The major challenge lies in the optimization of various deposition parameters to obtain NiTi film of near-equiatom composition combined

B. Geetha Priyadarshini (✉) · S. Aich · M. Chakraborty
Department of Metallurgical and Materials Engineering, Indian Institute of Technology, Kharagpur 721 302, West Bengal, India
e-mail: geethapriya@metal.iitkgp.ernet.in

M. Chakraborty
School of Mechanical Sciences, Indian Institute of Technology,
Bhubaneswar 751 013, Orissa, India

with high deposition rates ($\sim 1 \mu\text{m/h}$) and desired properties to tailor for specific applications such as microactuators [30].

At low pressure, simultaneous deposition of Ni and Ti films from individual magnetron source may lead to reduction in deposition rate of Ni films due to which variation in the composition of NiTi films may result. This is due to the fact that ferromagnetic materials cannot be efficiently sputtered nor can the plasma be ignited at low gas pressures if there is not sufficient magnetic flux intensity in front of the targets. DC-magnetron sputter deposition of ferromagnetic material leads to major difficulties, such as magnetic field is shunted through the nickel target and it is very difficult to form a closed loop of magnetic flux on the target surface [31, 32]. Chang et al. found the magnetic field strength is the key parameter in the DC-magnetron sputter-deposition of nickel films in particular to achieve high deposition rates [33].

Therefore, the motivation for the present study is to gather prerequisite knowledge on deposition rate, structure and morphology of independently grown nickel films deposited under wide range of sputter parameters for subsequent processing of Ni–Ti shape memory alloy films. Thus, systematic studies on the effects of deposition parameters such as target power, argon gas pressure, substrate-bias voltage and substrate temperature on the properties of Ni film are indispensable. It appears that, a detailed discussion based on this aspect of study has not been reported in literature so far. The present authors believe that the basis of this study on pure nickel films is a good model for the deposition of Ni/Ti films. In addition, the study of pure nickel films is of interest owing to different applications.

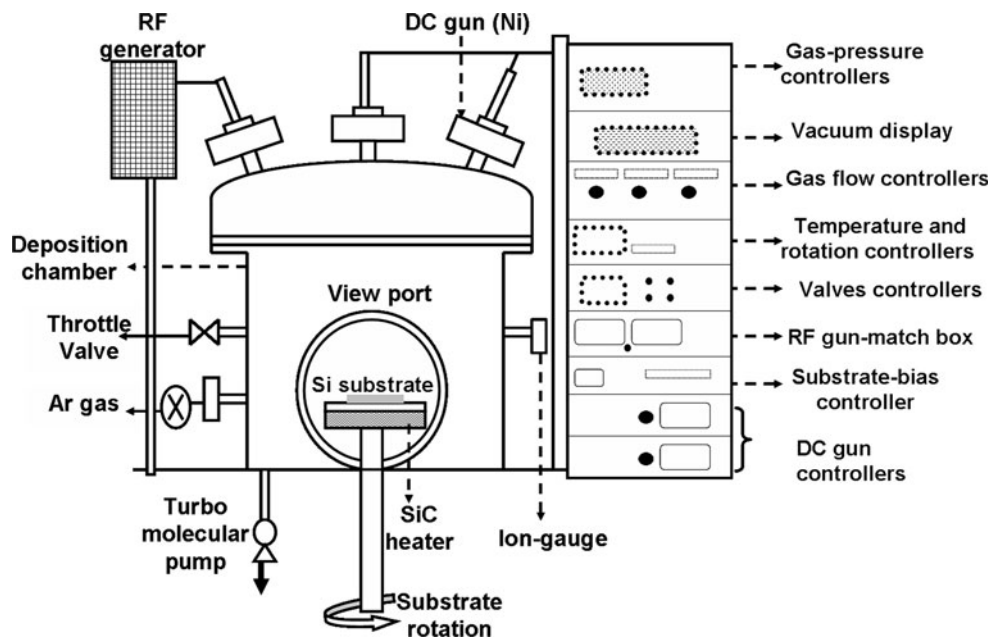
In the present work, nickel films have been deposited by conventional DC-magnetron sputtering on (100)-oriented single crystal silicon wafers. In diode-based sputtering systems, sputter parameters, *viz.*: argon gas pressure, substrate-target distance, substrate-bias voltage, and target power considerably influence the film deposition rate as well as the microstructure of the film. The rate of surface diffusion of adatoms on the substrate surface governs the film microstructure which is subjective to either substrate temperature or substrate-bias voltage applied during the sputter-deposition. Focus of the present work is, therefore, to study the effects of argon gas pressure, DC power, substrate-bias voltage and substrate temperature on the properties of nickel films. Systematic studies on the film microstructure and surface roughness were performed using field emission scanning electron microscopy (FE-SEM) and atomic force microscopy (AFM), respectively. Grazing incidence X-ray diffraction technique (GIXRD) was employed to study crystallinity, structure and texture of nickel thin film. The results from this combination of techniques have shed light on the film morphology, grain size, surface roughness, and orientation of nickel films.

Experimental details

Deposition of Ni films

All nickel films were deposited using an RF/DC-magnetron sputtering system (KVT Ltd) which is a three-gun “sputter-down setup.” A schematic representation of the deposition system is shown in Fig. 1. The sputter chamber was

Fig. 1 Schematic representation of sputtering system



evacuated to a base pressure lower than 3×10^{-6} Torr using turbo molecular pump driven by rotary pump. 99.9% pure Ni with diameter of 3 inches was employed as the sputter target. The argon gas of 99.99% purity was used as the sputtering gas with constant flow rate of 50 sccm. The chamber pressure was measured by ion-gauge and the argon gas pressure was controlled by the throttle valve. Sputter-deposition pressure was measured using MKS Baraton pressure gauge. Nickel films were deposited on to $3 \text{ cm} \times 3 \text{ cm}$ *P*-type Si (100) substrates which were ultrasonically cleaned with acetone and alcohol. Prior to the depositions, substrates were etched with 2% HF solution in order to remove native oxide layer on the surface. To ensure the purity of the films, pre-sputtering of nickel target for about 5 min was done to remove surface oxides. In order to maintain the uniformity in the film thickness the substrates were rotated at 10 rpm for all the depositions. The films were deposited with various DC sputtering power (W), deposition pressure (mTorr), substrate temperature ($^{\circ}\text{K}$) and substrate-bias voltage (V). The deposition details for four sets of experiments to study the influence of deposition pressure, sputtering power, substrate-bias voltage and substrate temperature on the deposition rate,

microstructure, and phase formations were tabulated in the Table 1.

Characterization of Ni films

Nickel film thickness ranging 50–400 nm was measured using step height on a masked silicon substrate using Veeco-Dektak 150 surface profilometer. RMS roughness of Ni films was obtained using the same surface profilometer. The film structure and morphology were studied by grazing incidence X-ray diffraction (GIXRD) and field-emission gun scanning electron microscopy (FE-SEM). The diffraction data were collected using Philips X'Pert diffractometer with Cu-target ($\lambda = 1.54056 \text{ \AA}$) which was employed to determine the crystalline phases generated. The grazing angle was fixed at 0.5° with scan step size of 0.05° over angle range of $2\theta = 30\text{--}100^{\circ}$. The tube was set to an accelerating voltage of 40 kV at a current of 30 mA. Studies on surface topography were carried out using Veeco-Nanoscope IV atomic force microscopy under tapping mode. Studies on microstructure and nature of film growth were done on both planar and cross-sectional nickel films by Carl Zeiss-SUPRA40 field-emission gun scanning

Table 1 Deposition details of Ni films

Exp.	Argon gas pressure (mTorr)	WD _{TS} (mm)	Power (W)	Substrate-bias (V)	Substrate temperature (K)	Deposition time (min)
Set 1						
P1	5	150	100	Unbiased	300	10
P2	10	150	100	Unbiased	300	10
P3	12.5	150	100	Unbiased	300	10
P4	15	150	100	Unbiased	300	10
P5	17.5	150	100	Unbiased	300	10
P6	20	150	100	Unbiased	300	10
P7	22.5	150	100	Unbiased	300	10
Set 2						
S1	5	125	50	Unbiased	300	10
S2	5	125	100	Unbiased	300	10
S3	5	125	150	Unbiased	300	10
S4	5	125	200	Unbiased	300	10
S5	5	125	250	Unbiased	300	10
S6	5	125	300	Unbiased	300	10
Set 3						
V1	10	150	100	−10	300	10
V2	10	150	100	−30	300	10
V3	10	150	100	−50	300	10
V4	10	150	100	−70	300	10
V5	10	150	100	−90	300	10
Set 4						
T1	20	150	300	Unbiased	570	30
T2	20	150	300	Unbiased	770	30

electron microscope with an acceleration voltage of 5 kV and a magnification up to 200 KX.

Results and discussion

Influence of deposition parameters on deposition rate

Figure 2 demonstrates the influence of various sputtering parameters on the Ni deposition rate. The film deposition rate is defined as the ratio of film thickness (measured by surface profilometer) to the deposition time. Equation 1 shows the dependence of film deposition rate on the sputtering variables [34]:

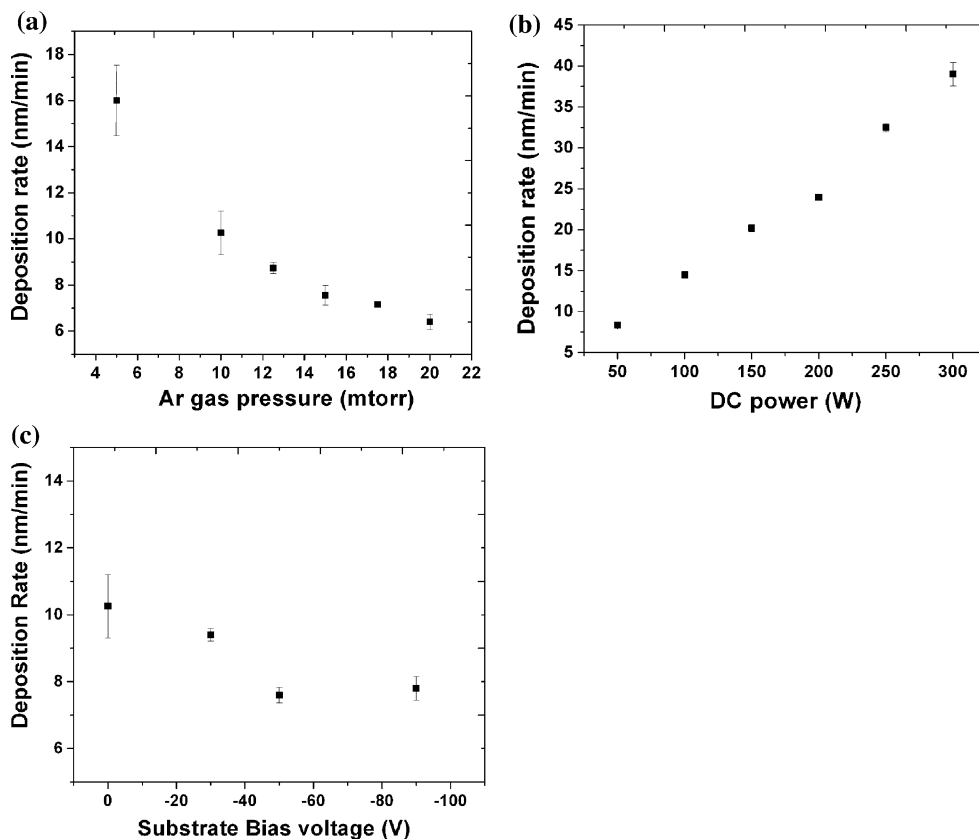
$$R = \frac{k \cdot P}{\rho \cdot d} \tag{1}$$

P is the power, ρ is gas pressure, d is electrode distance, and k being constant of proportionality, which is the function of type of gas and the target material employed. From Fig. 2a it can be observed that deposition rate decreases from 16 to 6.5 nm/min when the deposition pressure increases from 5 to 20 mTorr at constant DC power of 100 W. In principle, the increase in gas pressure favors excess number of argon gas species accompanied with shorter mean free-path which is defined as the mean

distance that a particle travels in a gas before encountering a collision with another gas molecule. According to kinetic theory of gases, the pressure (ρ) is inversely related to the mean free-path of the gas species (τ) [35]. This in turn contributes to the high collisional scattering events taking place between Ni atoms and argon gas species. Hence, some of the Ni atoms scatter away from the substrate, so the number of atoms depositing on the substrate decreases leading to low deposition rates. The fact that the decrease in deposition rate with higher gas pressure due to the shorter mean free path has been observed by few researchers in magnetron-sputtered Ga-doped ZnO [36] and SiC films [37]. Mikami et al. [38] had employed RF-DC coupled magnetron discharge to confine the efficient plasma near the magnetic target and deposited Ni films on both Si and corning glass substrates and found decrease of deposition rate with increase in gas pressure.

The deposition rate for the Ni films deposited at various DC power are plotted in the Fig. 2b. It has been observed that the Ni sputter-deposition rate increases linearly with the DC power. This can be explained considering Eq. 1, which shows the linear dependence of target power with the film deposition rate. Further, this kind of dependence of deposition rate on sputtering power can be elucidated on the basis of DC voltage (V_{dc}) applied to the target during

Fig. 2 Deposition rate as a function of **a** Argon gas pressure, **b** DC power and **c** Substrate-bias voltage, for Ni films deposited at room temperature



sputter deposition. In magnetron discharge systems, the target-current density (J_d) is related to the applied DC voltage at cathode (V_{dc}) and is given by Child-Langmuir law [35, 39];

$$J_d = \frac{4\epsilon_0}{9} \sqrt{\frac{2e}{M}} \frac{V_{dc}^{3/2}}{r^2} \quad (2)$$

ϵ_0 is the space permittivity, e and M is the charge and mass of the electron, r is the larmor radius (eV). Argon ion flux and its average kinetic energy (KE_{av}) upon striking the target which are functions of applied DC voltage are the two major factors which govern the sputtering rate from the target (refer Eqs. 2 and 3).

$$KE_{av} \propto V_{dc} \quad (3)$$

It is now evident that high argon ion flux not only results in argon ion with high kinetic energy, but also increases the probability of ejection of target atoms with substantial ion bombardment on the target. The above stated mechanisms are proportional to applied DC voltage (sputtering power) and hence contribute to the increase of Ni sputter-deposition rate. Similar dependence relationship between deposition rate and target power was also reported in sputtered Cu films on Si (100) [40].

Figure 2c shows the variation of deposition rate with substrate-bias voltage at constant DC power of 100 W and argon gas pressure of 10 mTorr. The deposition rate decreased from 10.3 to 7.8 nm/min when the negative substrate-bias voltage was increased from 0 to -50 V. However, at -90 V, substrate-bias voltage the deposition rate was found to be constant at 7.8 nm/min. This indicates that on application of small negative bias to the substrate, the low energy positive argon ion species are attracted towards the substrate and thus sputter-off the growing film surface. This could have caused a slight decrease in the film thickness and hence, the Ni sputter-deposition rate. Further, upon increasing the bias voltage there might be enhanced re-sputtering of depositing species from the film surface which may result in considerable lowering of deposition rate.

Influence of deposition parameters on the surface roughness and film topography

Studies related to film roughness and surface topography are essential for almost any sort of coating applications. Since these determines the various properties of the coating such as electrical, mechanical, optical corrosion resistance, etc. In the present study, the surface topography of Ni films is found to be greatly affected by the deposition parameters and corresponding RMS film roughness values were obtained by using stylus surface profilometer. Figure 3a shows the plot for Ni film roughness grown at various

argon gas pressures on Si substrate at room temperature. RMS roughness was found to decrease from 5 to 1.25 nm as the gas pressure was increased from 5 to 17.5 mTorr, for pressure above 17.5 mTorr the roughness increases again. This behavior can be understood in view of shorter mean free path of argon gas species at high deposition pressure. It is important to point out that, the average kinetic energy of Ni adatoms decreases due to the enhanced collisional event taking place between sputter Ni atoms and argon gas species resulting in a broader angular distribution of the particles on the Si substrate. Thus, the decrease in surface mobility of adatoms coupled with high nucleation density leads to the formation of finer Ni grains leading to smoother surface [41]. The increase in roughness beyond 17.5 mTorr could be attributed to the increase in the density of void boundaries present in the films. The increase in the density of void boundaries with argon gas pressure will be discussed in the forthcoming sections.

As shown in Fig. 3b, the surface roughness values of Ni films decreased as the substrate-bias voltage was increased from -10 to -50 V. Beyond -50 V, the film tends to show slight increase in the surface roughness value. This behavior is predicted due the improvement in the surface diffusion of adatoms during application of moderate substrate bias which eventually leads to low film roughness accompanied with dense and compact structure. With increase in the bias voltage up to -50 V causes ion bombardment on the growing film surface which generally results in filling up of void boundaries by surface migration of adatoms leading to smooth continuous film. On the other hand, the increase of bias voltage beyond -50 V tend to show rougher Ni films which might be due to the enhanced ion-bombardment on the growing film surface leading to the re-sputtering and thereby inducing defects in the film [42].

Figure 3c demonstrates the dependence of Ni film roughness on the deposition power. It is observed that the roughness of Ni film increases from 4 to 12 nm as the sputtering power was increased from 50 to 300 W. This can be explained considering that the film thickness increases as the DC power is increased which would result in a larger Ni grains. In addition, surface mobility of adatoms increases at high DC power which leads to crystalline films. To further support the argument that the roughness increases with DC power as demonstrated in Fig. 3c, the plot of Ni film roughness as function of film thickness is plotted in Fig. 4 at varied DC power ranging from 50 to 300 W. The significant implication which can be drawn is that low RMS roughness can be achieved for thin Ni films when they are deposited at low DC power compared to high DC power. Thus, it can be attributed that the increase in DC power enhances adatom number density with sufficient adatom mobility which contributes to the coalescence

Fig. 3 Surface roughness as a function of **a** Argon gas pressure, **b** Substrate-bias voltage and **c** DC power, for Ni films deposited at room temperature

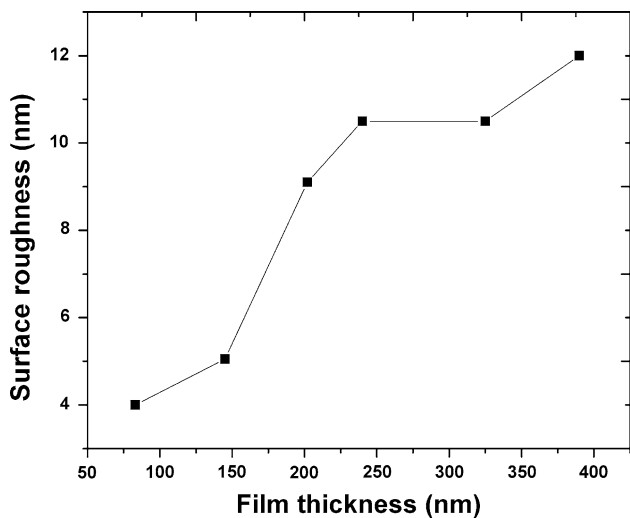
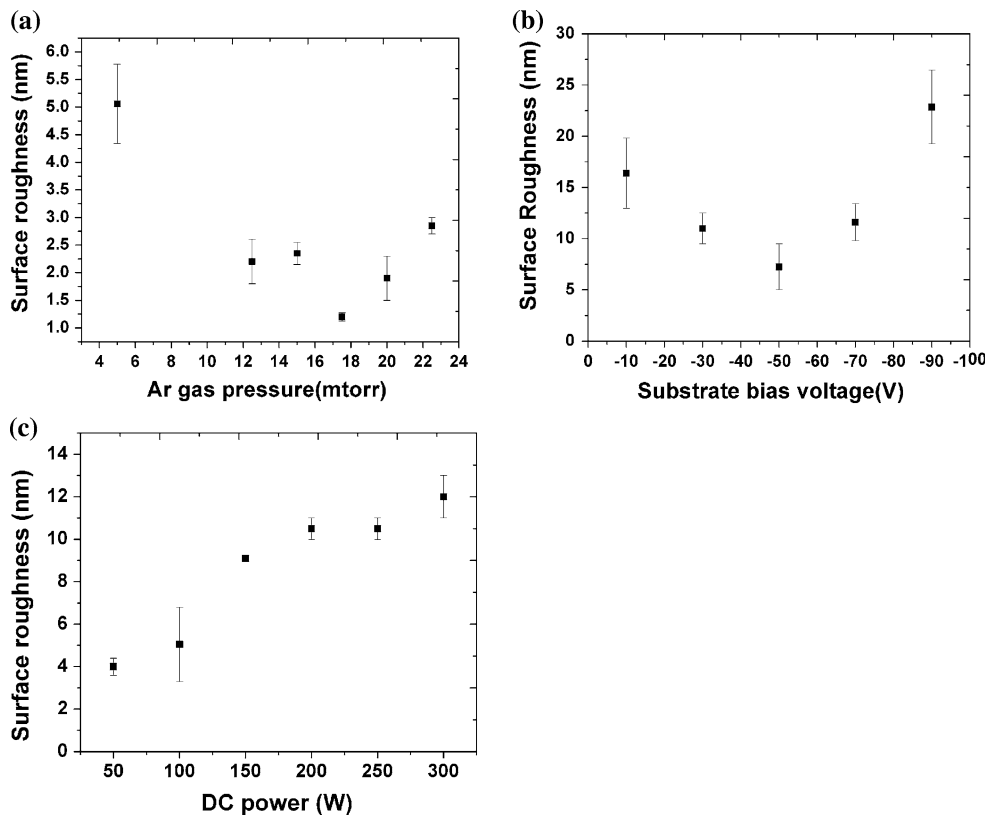


Fig. 4 Film surface roughness as a function of film thickness

of grains. However, it is also worth mentioning that the present case involves deposition of high melting point material on substrates (at room temperature) hence, the surface mobility of condensing atoms governs the density of void boundaries as well as the surface roughness.

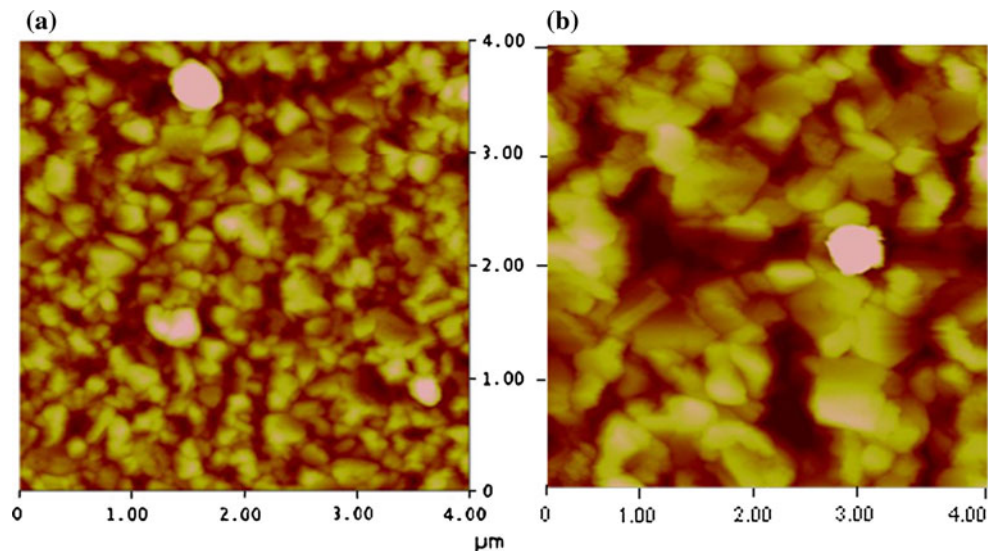
To investigate the effects of substrate temperature on the surface topography and roughness of Ni films, AFM analysis was carried out on Ni films. Figure 5a and b shows the AFM images of the Ni films deposited on Si substrates

held at 570 and 770 K, respectively. The images were acquired in a $4 \mu\text{m} \times 4 \mu\text{m}$ scan area. It is evident from the AFM images that the grain size increases in addition to the increase in surface roughness from 10 to 23 nm as the substrate temperature was increased from 570 to 770 K. The variation in surface topography with substrate temperature is the consequence of grain growth taking place. When films are sputter-deposited on substrates held at high temperature, there is substantial increase in the rate of surface migration of adatoms on the substrate surface. This is due to fact that the adatoms gain additional energy apart from the kinetic energy and while they reach the growing film surface, result in promotion of larger grains due to the coalescence of neighboring grains. Hence, it is believed that the increase in film roughness is probably due to the increase in the lateral grain size occurring in the film at high substrate temperature. This behavior is in accordance with the work reported by Musil et al. which pointed out that the film roughness is induced by the film crystallization which in turn controls the energy delivered to the growing film [43].

Influence of deposition parameters on film crystallinity and texture

Mechanical and functional properties of thin film are significantly affected by structure and orientation of grains in

Fig. 5 AFM images of Ni films deposited at **a** 570 K and **b** 770 K substrate temperature



deposited film. Preferred orientations in the films are greatly influenced by deposition method, variables, nature of the substrate, energetic ion bombardment, and geometrical confinement by surface features. Among these, deposition parameters are known to be the major contributing factors for the development of texture in a film. All the XRD spectra were obtained in the grazing incidence mode where the X-ray glances over the surface of Ni film without penetrating deep inside the substrate. Because of this reason, none of the XRD spectra shows the presence of Si peaks despite of low Ni film thickness. Figure 6a shows the GIXRD patterns for Ni films deposited at argon gas pressures of 10 mTorr (120 nm thick), 12.5 mTorr (94 nm thick), and 15 mTorr (71 nm thick) on Si substrate at room temperature with deposition power of 100 W. It was found that all the Ni films crystallized in the face-centered cubic (fcc) $Fm\bar{3}m$ phase and the crystallites were oriented along the (111) plane. This indicates the films exhibit a preferred (111) grain orientation parallel to the film surface which is typical for fcc metal films. It is also evident that the texturing of Ni films along (111) plane was more pronounced when deposited at low deposition pressure and the relative portion of (111) intensity gradually decreases with increase in argon gas pressure to 15 mTorr. In order to obtain a deeper insight into the influence of argon pressure on the grain size (G), well-known Scherrer's formula was employed to calculate the grain size from (111) diffraction peak:

$$G = \frac{0.9\lambda}{FWHM \cdot \cos \theta} \quad (4)$$

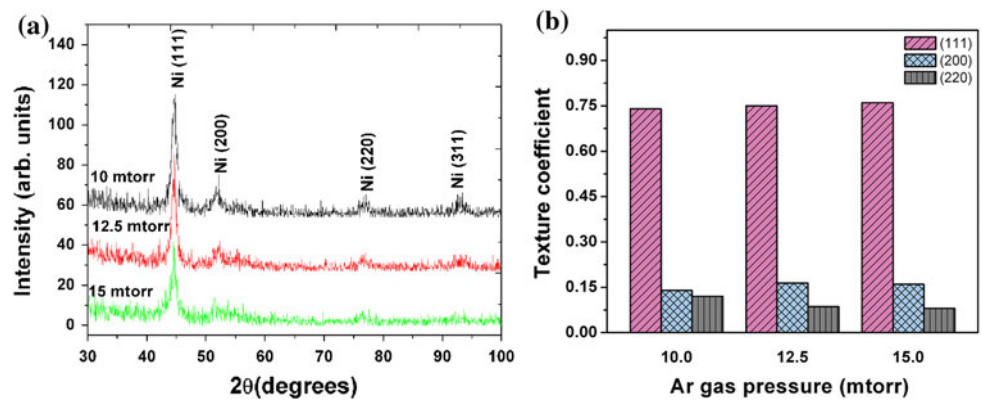
λ is the X-ray wavelength, $FWHM$ is the full-width half-maximum of the diffraction peak, and θ is the diffraction angle. The crystallite size was calculated using Eq. 4 and was found to decrease from 10 to 6 nm with increase in

argon gas pressure from 10 to 15 mTorr (see Table 2). Igasaki and Kanma had observed decrease in grain size of ZnO:Al films deposited on glass substrate with increase in the working pressure and attributed to increase in grain boundary area [44]. Our result suggests that due to enhanced collision scattering between target atoms and argon gas species at high gas pressure, lead to reduced adatom mobility on the substrate surface tending to form Ni film with low crystallinity. Therefore, reduced surface mobility of adatoms causes incapability of aggregation of individual islands at high deposition pressure leading to smaller grain size. Such result has also been observed by Assuncao et al. in Ga-doped ZnO films [36] and by Cheng et al. in AlN film [45]. These authors also suggests that low surface diffusion of the sputtered species after collisions at high deposition pressure lead to less crystalline films

Table 2 Influence of deposition parameters on crystallite size of Ni films

Sample No.	Deposition parameter	Crystallite size (nm)
P2	10 mTorr	10
P3	12.5 mTorr	9
P4	15 mTorr	6
S1	50 Watts	5
S4	100 Watts	9
S6	300 Watts	15
V1	0 V	10
V2	−30 V	10
V3	−50 V	–
V5	−90 V	11
T1	570 K	18
T2	770 K	33

Fig. 6 GIXRD patterns and texture coefficient of Ni films deposited on Si substrate at room temperature **a** and **b** as a function of working pressure indicated on the each pattern



accompanied with grain size reduction. The texture coefficients (T) of Ni films deposited on Si substrates as a function of argon gas pressure are calculated from the corresponding XRD peaks using the following formula [46].

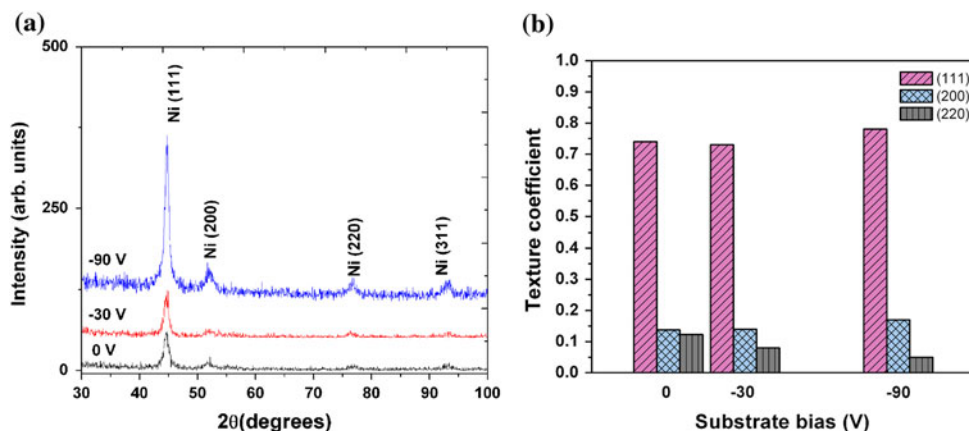
$$T = \frac{I(hkl)}{I(111) + I(200) + I(220)} \quad (5)$$

where (hkl) are (111), (200) or (220) orientations and I is the relative intensity. It can be observed from Fig. 6b that the texture coefficient is influenced by the argon gas pressure. From the XRD pattern (Fig. 6a) it is also noticed that the intensity of (111) peak decreases with increase in gas pressure which is supported by the lowering of (111) texture coefficient as shown in Fig. 6b. Although, a slight reduction in the film thickness cannot be substantiated for such lowering of (111) texture coefficient at higher deposition pressure. Further, it is found that the dominant (111) orientation becomes a preferred orientation even at 15 mTorr argon gas pressure. It is reported that in case of fcc materials, the grains with (111) planes parallel to the film surface will have minimum surface and interface energy due to high density of packing in (111) plane [47]. Therefore, adatoms with higher energy are energetically favorable for the formation of (111) surface planes and contribute to $\langle 111 \rangle$ fiber texture. Ni films deposited at 10 mTorr gas pressure exhibits a mixture of (111), (200) and (220) orientations. However, at high gas pressure (200), texture coefficient was found to increase among the (111), (200) and (220) orientations, whereas (220) intensity was reduced. This suggests that the high deposition pressure improves the growth of (200) plane along with (111) preferred orientation.

Figure 7a shows the GIXRD pattern for Ni films deposited at 0 V (120 nm thick), -30 V (93 nm thick), and -90 V (76 nm thick) substrate-bias voltage on Si substrate at room temperature with DC power 100 W and 5 mTorr gas pressure. Increase in film crystallinity accompanied with improvement in texture was observed in Ni films with increase in the negative bias voltage. XRD profile of Ni

film deposited at -90 V bias shows a distinct (111) preferential orientation, while rest of the peak are insignificant, which is characteristic of $\langle 111 \rangle$ fiber texture in the film. The differences between these Ni films are the bombarding energy of the deposited particles and film thickness. However, the Ni films deposited at -90 V tend to exhibit high relative (111) peak intensity, in spite of low film thickness when compared to the Ni films deposited at 0 and -30 V. This suggests that the film thickness has insignificant effect on the film texture provided energy of bombarding species plays a vital role on the texture development. The improvement in the intensity of (111) reflection with substrate-bias voltage as observed in Fig. 7a can be explained from the viewpoint of the surface energy and kinetic factors. Due to small negative bias at the substrate end during sputter deposition, argon ions accelerate towards the substrate with moderate energies. These ions upon bombardment on the substrate translate part of their kinetic energy to the adatoms and hence improve the surface diffusivity, leading to more crystalline films [48]. The observation of distinct (111) texture in Ni films deposited at -90 V is similar to the $\langle 111 \rangle$ fiber texture obtained from electron diffraction ring pattern of room temperature deposited Ni film grown at -100 V bias voltage on NaCl substrates by Mitra et al. [47]. It is important to point out here that few authors have observed lowering of crystallinity from the diffracted intensity (texture) in fcc metal films like, Ag [49] and Ni [47] even at higher bias voltage as compared to those films grown at a lower or no bias. They suggested the reason behind the degradation of film crystallinity was due to the excessive adatom mobility at higher bias voltage which led to re-sputtering and re-crystallization. Further, it is observed that there is no significant increase in the crystallite size of the Ni film as the bias voltage from 0 to -90 V (see Table 2). Therefore, effect of ion bombardment during sputter deposition on grain size of the films is insignificant in the present case. With varying substrate-bias voltage (Fig. 7b), the Ni films revealed (111) orientation of higher texture coefficient irrespective of unbiased and biased condition. The texture

Fig. 7 GIXRD patterns and texture coefficient of Ni films deposited on Si substrate at room temperature **a** and **b** as a function of substrate-bias voltage indicated on the each pattern

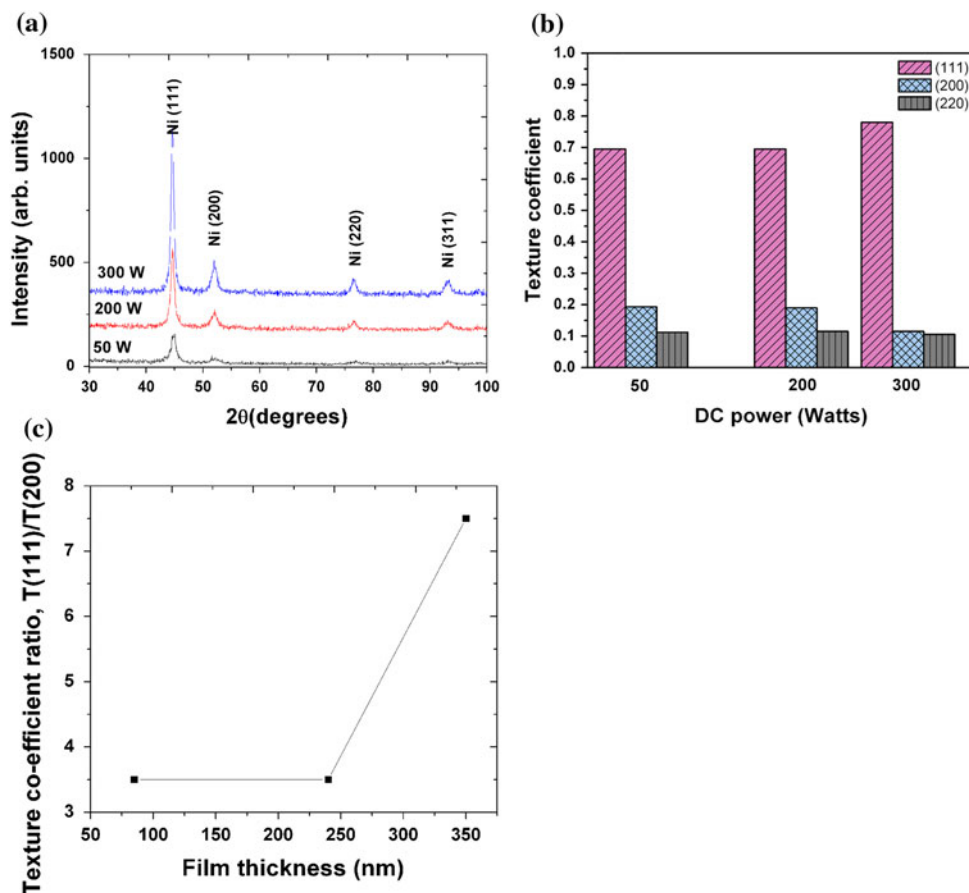


coefficient of (111) orientation in Ni film deposited at substrate bias of -90 V is highest amongst the films deposited at 0 V and -30 V. In addition (200) intensity was found to increase along with the (111) preferred orientation. This depicts that enhanced surface mobility of the adatoms due to the impingement of low energy ions on the substrate surface leads to random orientation of the grains leading to polycrystalline Ni films.

The GIXRD patterns for Ni films deposited at 50 W (85 nm thick), 200 W (240 nm thick) to 300 W (350 nm thick) DC powers on Si substrates held at room

temperature are shown in Fig. 8a. The diffraction pattern shows the polycrystalline nature and the films are indexed to face-centered cubic $Fm\bar{3}m$ Ni phase. Ni films deposited at 50 W are found to be weakly textured in (111) plane. As the power was raised to 300 W, the intensity of (111) plane was found to improve retaining a dominant (111) fiber texture. This is attributed to the increase in the film thickness with increase in the DC power. The number density of sputtered species increases due to increase in the amount of argon ion flux contributing to the high probability of sputtering event. Chan et al. [50] observed highly

Fig. 8 Ni films deposited on Si substrate at room temperature **a** GIXRD patterns, **b** Texture coefficient and **c** Texture coefficient ratio as a function of film thickness



crystalline DC-magnetron-sputtered Cu films at high power and suggested that the surface mobility of adatoms increases due to high kinetic energy gained by depositing species, which are responsible for the formation of highly crystalline film. Further, grain size is found to increase from 5 to 15 nm as the DC power was increased from 50 to 300 W (see Table 2). At high DC power, argon ion flux increases which strikes the Ni target with enormous energy. During the process, momentum transfer takes place causing ejection of target atoms with high kinetic energies. The Ni adatom upon striking the substrate surface has now gained sufficient energy to migrate on the surface and thereby coalesce to form larger grains. The texture coefficient is greatly affected by the DC power and is shown in Fig. 8b. At low DC power, the dominant (111) orientation becomes a preferred orientation. However, at 300 W DC power the (111) texture coefficient was increased among the (111), (200) and (220) orientations, whereas that of (200) intensity is reduced. Hence, it can be understood that higher DC power favors the orientation of grains in (111) and (220) planes when compared to the low DC power. Figure 8c depicts the variation of texture coefficient ratio (T_{111}/T_{200}) as function of film thickness. For film thickness 75–240 nm there is no change in the value of texture coefficient ratio. At film thickness of 350 nm the ratio is found to increase drastically suggesting that the grains of Ni thin films evolve to (111) direction with increasing thickness and that the (111) planes have the lowest surface energy.

GIXRD pattern for the Ni films deposited at 570 and 770 K substrate temperatures are shown in the Fig. 9a and b, respectively. Even the Ni films deposited at high substrate temperature favors the texturing of grains in [111] direction. However, the GIXRD pattern for Ni films does not show any signature of nickel silicides' formations, which are likely to form at high substrate temperature near the film/substrate interface. This is probably due to the insufficient energy of Ni adatom to undergo the process of bulk diffusion into the Si substrates. The grain size of the films was calculated by using Eq. 4 and it was found to increase from 18 to 33 nm for the Ni films as the deposition temperature was raised from 570 to 770 K. Such result has also been reported by Chawla et al. in case of Ti films and suggested that the increase in the surface and grain boundary diffusivity of adatoms causes the grain growth at high substrate temperature leading to the increase in the grains' size and roughness [46]. This discussion seems to be relevant in the present case too. It should also be noted that the normal grain growth is not expected in thin films. Instead, abnormal grain growth takes place often leading to bimodal grain size distribution caused by secondary grain growth in which some grains may grow excessively large relative to surrounding ones [35].

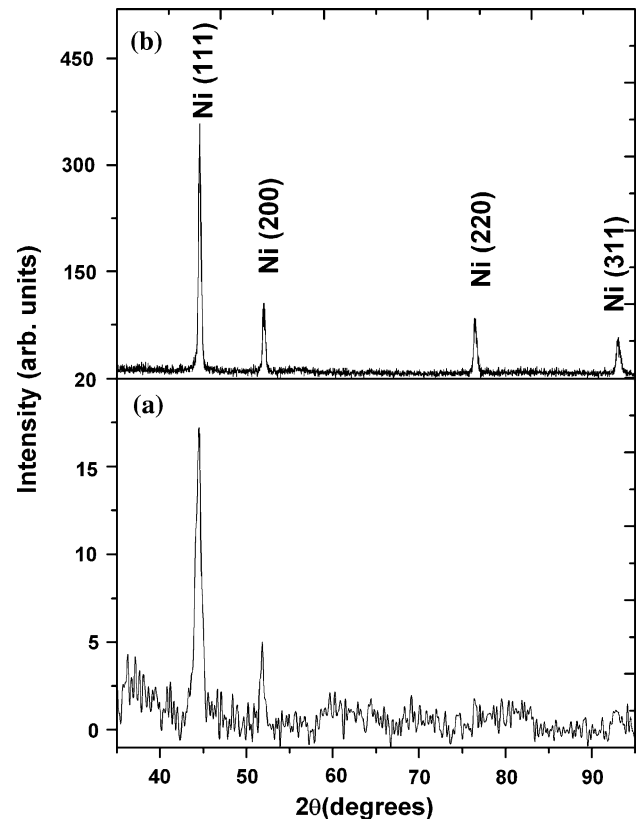


Fig. 9 GIXRD pattern of Ni films deposited at **a** 570 K and **b** 770 K substrate temperature

Influence of deposition parameters on film morphology

Figure 10a–c shows the FE-SEM micrographs of Ni films deposited at different argon gas pressures. The micrographs clearly indicate the increase in density of cracks as the deposition pressure was increased from 10 to 20 mTorr. On closer observation, the film microstructure comprises very fine grains separated by void boundaries. An extensive study by Thornton [51] on the structure-zone model (SZM) of sputtered films revealed that the oblique component of the deposition flux is responsible for more open-type void boundaries. This is because of enhanced collision scattering between the argon ions and target species surpass the effect due to the adatom mobility for depositions at high gas pressure. Therefore, in the present case the increase in density of void boundaries is accounted due to the self-shadowing effect of individual islands which takes place during the film condensation-growth process. The adatoms impinge on the substrate randomly due to high scattering, and areas such as valleys are not completely filled up. Thus the tendency of growth of islands increases in the vertical directions instead of lateral directions due to insufficient atomic mobility on the substrate surface. This result is comparable with the film roughness, which was previously

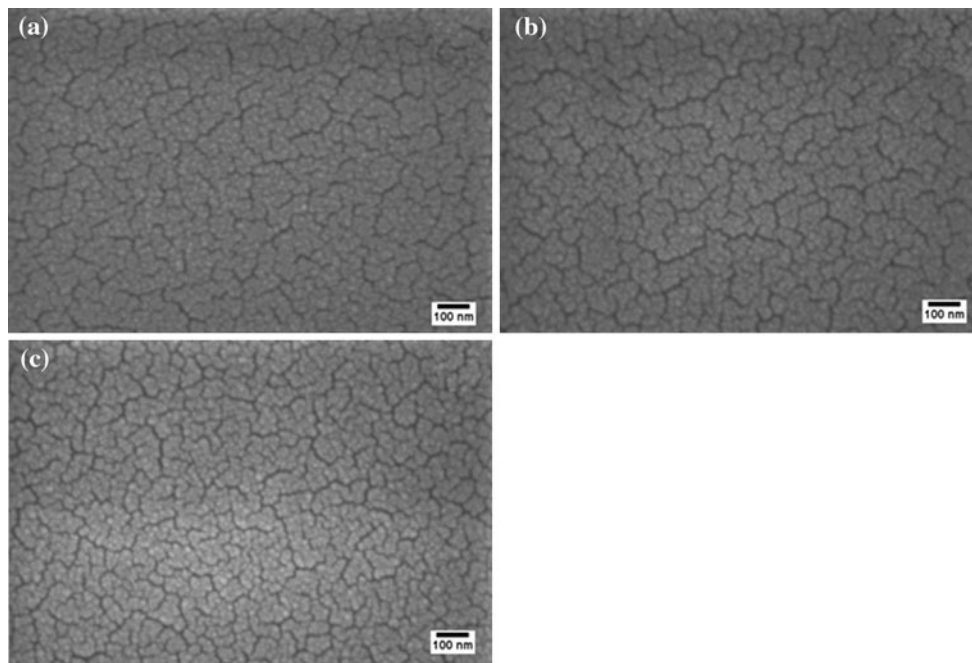


Fig. 10 Planar FE-SEM images of Ni films deposited at **a** 10 mTorr, **b** 15 mTorr and **c** 20 mTorr

found to increase beyond 17.5 mTorr gas pressure due to the presence of high density of void boundaries.

Figure 11a, c and e shows the FE-SEM planar images of Ni films deposited at 50 W, 200 W and 300 W on Si substrate at room temperature with deposition pressure of 5 mTorr. The Ni films exhibit the crack-like microstructure irrespective of increase in the sputtering power. At low sputtering power, adatoms with low kinetic energies result in negligible surface migration (see Eq. 4). In such case the morphology of films is often observed to be non-continuous with frequent void boundaries. However, Ni film deposited at DC power of 300 W was found to contain lower density of cracks accompanied with long, continuous and wider void boundaries. This can be explained on the basis of nucleation and growth of thin films, the islands try to merge with other islands leaving long-continuous and wider void boundaries depicting the densification of film which occurs during film growth process. Figure 11b, d, and f shows the cross-sectional FE-SEM images of Ni films deposited at different DC power. Ni film deposited at low sputtering power exhibit columnar structure with porous space separating in between (Fig. 11b). This can be further correlated to the zone I structure of SZM [52, 53] for sputtered films at low T_s/T_m (T_s is the substrate temperature and T_m is the melting temperature of target material). Limited surface diffusion of adatoms on the substrate surface is attributed to the formation of such columnar structure as observed in Fig. 11b. Another reason could be due to the direction of incident beam flux on the substrate

surface during the deposition. When the impingement of incident beam flux is in oblique direction, the presence of high points on the substrate surface set a pathway to receive maximum flux rather than the valleys which receive less amount of incident flux. This difference causes the growth of individual islands comprising columnar structure with void boundaries. However, as the sputtering power was raised to 300 W the film displays long, dense fine fibrous columnar structure having column width of ~ 50 nm (Fig. 11f). Deposition of Ni films at higher sputtering power involves high kinetic energies of adatoms leading to the enhanced surface migration on the substrate surface contributing to poorly defined-fibrous columnar structure (zone T structure).

Application of substrate bias during sputter deposition has been proven to be an efficient means to modify the microstructure of the growing film and thus its properties [35, 54–56]. Ion bombardment during sputter deposition causes surface modification of films deposited at room temperature yielding high surface diffusion of adatoms. Surface modification of film during ion striking on the film may lead to the following: desorption of weak bonds, reflection of energetic species (adatoms, ions or neutrals), re-sputtering from the film, introduction of imperfections, enhanced surface diffusion of adatoms. Figure 12a and c reveals the planar FE-SEM micrographs of the Ni films deposited under substrate-bias voltage of -10 and -90 V, respectively. From the micrographs, it is evident that application of substrate-bias voltage leads to the

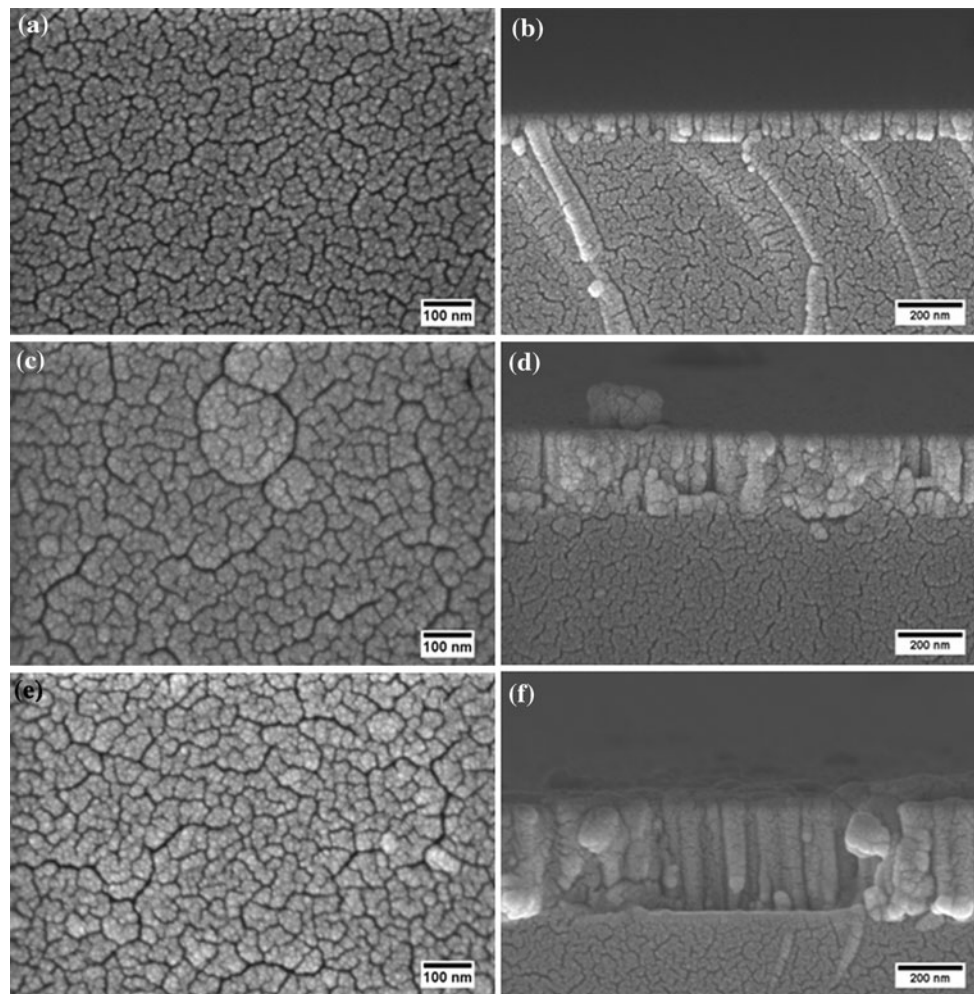


Fig. 11 Planar and cross-sectional FE-SEM images of Ni films on Si substrates for DC power. **a** and **b** 50 W, **c** and **d** 200 W and **e** and **f** 300 W

elimination of void boundaries leading to dense and smoother film surface. As previously observed, the decrease in the roughness value of Ni film deposited at -90 V is attributed to the reduction in density of voids. Further, Fig. 12b and d shows the cross-section FE-SEM images of Ni films deposited at substrate-bias voltage of -10 and -90 V, respectively, and it is confirmed that the substrate bias has insignificant effect on the film thickness. However, slight modification in the film structure from columnar structure (at -10 V) to smooth structure (at -90 V) can be observed. When negative bias voltages are applied to the substrate w.r.t. target during deposition, the low energy argon ions etch the silicon substrate as well as the growing film creating new nucleation sites and causing high adatom migration during film growth process. As a result, the breakage of columnar structure on the substrate occurs due to “knock-out” by high energy adatoms into the nearby valleys. Hence, the surface mobility of adatoms is greatly enhanced with considerable reduction in void

boundaries leading to more continuous and denser film morphology.

The crack-like microstructure which was previously observed in as-deposited Ni films was not present in Ni films deposited on Si substrate held at 570 K (Fig. 13a). At substrate temperatures of 570 and 770 K, the T_s/T_m ratio of Ni films was calculated to be 0.33 and 0.45, respectively. The ratio lies in the zone T (transition zone) and zone II of Thornton’s SZM and the expected microstructure is a large columnar structure with densely packed grain boundaries without void spaces [29]. The atomic mobility on the substrate surface increases, thereby adatom condensation occurs preferentially at the surface concavities leading to the smoother surface and denser Ni film. Figure 13b shows the cross-sectional FE-SEM microstructure of Ni films deposited at substrate temperature 770 K. A near-equiaxed grain structure with densely packed microstructure comprising large lateral grain size was observed. This indicates the high surface mobility of adatoms during the deposition

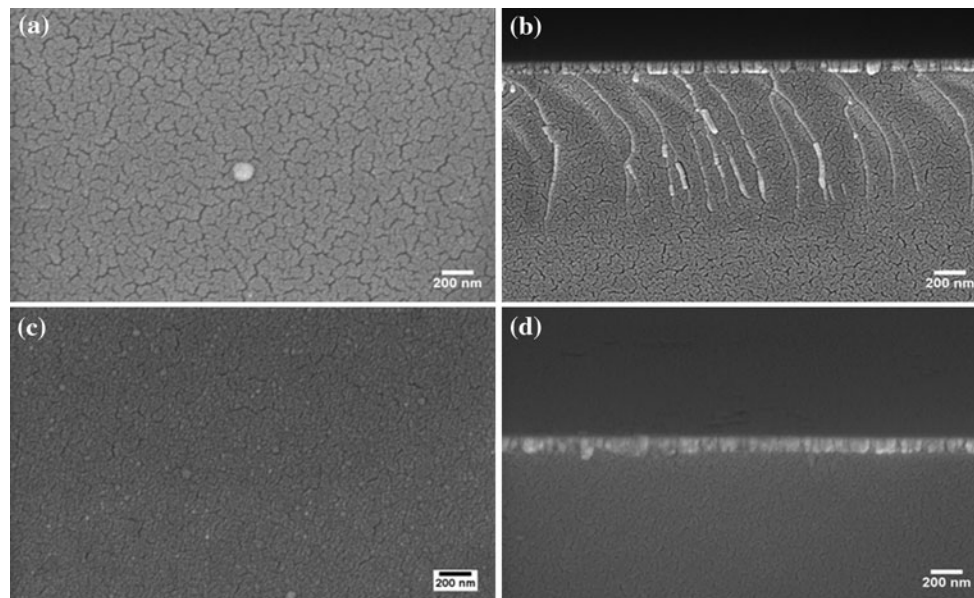


Fig. 12 Planar and cross-sectional FE-SEM images of Ni films deposited at **a** and **b** -10 V and **c** and **d** -90 V substrate-bias voltage

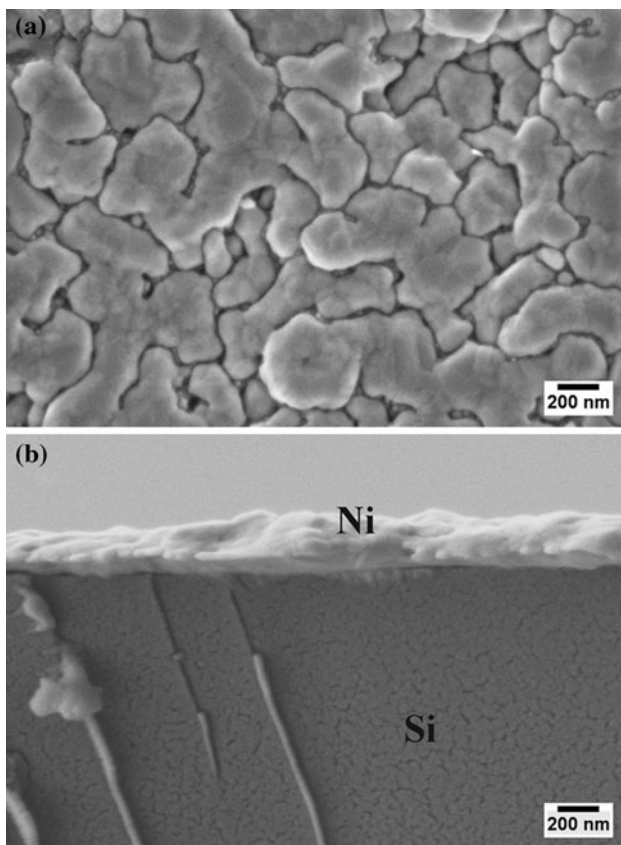


Fig. 13 FE-SEM image of Ni film deposited at **a** 570 K (planar) and **b** 770 K (cross-sectional) substrate temperature

on substrate surface leads to near-zone III type of structure. This type of film microstructure shows the clear evidence of film formation by Stranski–Krastanov model which is

layer-by-layer growth in addition to the island growth mechanism [35]. It is believed that the involvement of high activation energy in the process of thermal diffusion of adatoms at high substrate temperature compared to the process of condensation of adatoms in the as-deposited condition contribute to the formation of near-equiaxed Ni grain structure.

Conclusions

Nickel films have been successfully produced with high deposition rates (~ 40 nm/min) by DC-magnetron sputtering system at low pressure of 5 mTorr and target power of 300 W. The structural and morphological properties of Ni films deposited on Si (100) substrates were investigated as a function of argon gas pressure, target power, substrate-bias voltage, and substrate temperature. The results are encapsulated as follows:

1. All nickel films have mixed crystalline orientation of [111], [200], and [220] in the direction of film growth. Due to the high packing density of atoms in (111) plane in the case of fcc materials Ni film exhibit strong $\langle 111 \rangle$ fiber texture irrespective of various sputtering parameters.
2. The crystallite size ranging from 6 to 20 nm is observed in room temperature deposited nickel films, which extends the scope for processing of nanocrystalline nickel films with superior mechanical properties. However, with increase in the substrate temperature grain size found to increase from 18 to 33 nm.

3. The morphology of Ni films was found to be greatly influenced by the deposition parameters. In particular Ni films deposited at substrate-bias voltage of -90 V, exhibit void-free structure in comparison to unbiased film.
4. Ni deposition in presence of ion bombardment and high substrate temperature enhances the surface diffusion of adatom on the substrate surface leading to smooth, dense, crack-free microstructures with near-equiaxed microstructure possessing strong $\langle 111 \rangle$ texture.

Acknowledgements This research was supported by Indian Institute of Technology, Kharagpur, India. The authors would like to thank Prof. R. Mitra of Indian Institute of Technology, Kharagpur for his helpful comments and suggestions.

References

1. Kawabata K, Tanaka T, Kitabatake A, Yamada K, Mikami Y, Kajioaka H, Toiyama K (2001) *J Vac Sci Technol A* 19:1438
2. Gambino JP, Colgan EG (1998) *Mater Chem Phys* 52:99
3. Tam PL, Nyborg L (2009) *Surf Coat Technol* 203:2886
4. Avendano A, Azens A, Niklasson GA, Granqvist CG (2007) *Mater Sci Eng B* 138:112
5. Ai L, Fang G, Yuan L, Liu N, Wang M, Li C, Zhang Q, Li J, Zhao X (2008) *Appl Surf Sci* 254:2401
6. Zhang H, Zhou YN, Sun Q, Fu ZW (2008) *Solid State Sci* 10:1166
7. Nakai H, Qiu H, Adamik M, Safran G, Barna PB, Hashimoto M (1995) *Thin Solid Films* 263:159
8. Yang J, Makihara K, Nakai H, Hashimoto M, Barna A, Barna PB (1998) *Thin Solid Films* 319:115
9. Yang Y, Qiu H, Chen X, Yu M (2009) *Appl Surf Sci* 255:6226
10. Pauleau Y, Kukielka S, Gulbinski W, Ortega L, Dub SN (2006) *J Phys D Appl Phys* 39:2803
11. Yin Y, Pan Y, Rubanov S, Bilek MMM, McKenzie DR (2009) *Nanosci Nanotechnol Lett* 1:32
12. Tu KN, Mayer JW (1978) In: Poate JM, Tu KN, Mayer JW (eds) *Thin films inter-diffusion and reactions*. John Wiley, New York
13. Chiu KCR, Poate JM, Feldman LC, Doherty CJ (1980) *Appl Phys Lett* 36:544
14. Jardim PM, Acchar W, Losch W (1999) *Appl Surf Sci* 137:163
15. Bhaskaran M, Sriram S, Mitchell DRG, Short KT, Holland AS, Mitchell A (2009) *Micron* 40:11
16. Okassi S, Moulet JS, Lay S, Hodaj F (2009) *Microelectron Eng* 86:397
17. Bendahan Marc, Canet Pierre, Seguin Jean-Luc, Carchano Herve (1995) *Mater Sci Eng B* 34:112
18. Chen JZ, Wu SK (1999) *Thin Solid Films* 339:194
19. Chen P, Ting JM (2001) *Thin Solid Films* 398–399:597
20. Ishida A, Sato M (2003) *Acta Mater* 51:5571
21. Ho KK, Carman GP (2000) *Thin Solid Films* 370:18
22. Fu Y, Du H, Huang W, Zhang S, Hu M (2004) *Sens Actuators A* 112:395
23. Setton M, Van der Spiegel J, Rothman B (1989) *J Mater Res* 4:1218
24. Lehnert T, Tixier S, Boni P, Gotthardt R (1999) *Mater Sci Eng A* 273–275:713
25. Cho HHY, Kim HY, Miyazaki S (2006) *Mater Sci Eng A* 438–440:699
26. Krulevitch P, Ramsey PB, Makowiecki DM, Lee AP, Northrup MA, Johnson GC (1996) *Thin Solid Films* 274:101
27. Ohta A, Bhansali S, Kishimoto I, Umeda A (2000) *Sens Actuators A* 86:165
28. Sanjabi S, Cao YZ, Sadrnezhad SK, Barber ZH (2005) *J Vac Sci Technol A* 23:1425
29. Inoue S, Sawada N, Namazu T (2009) *Vacuum* 83:664
30. Fu YQ, Luo JK, Flewitt AJ, Huang WM, Zhang S, Du HJ, Milne WI (2009) *Int J Comput Mater Sci Surf Eng* 2:208
31. Iseki T, Maeda H, Itoh T (2008) *Vacuum* 82:1162
32. Zhang H, Poole J, Eller R, Keefe M (1999) *J Vac Sci Technol A* 17:1904
33. Chang SA, Skolnik MB, Altman C (1986) *J Vac Sci Technol A* 4:413
34. Zendeenam A, Ghanati M, Mirzaei M (2007) *J. Phys.: Conference Series* 61:1322
35. Ohring M (1991) *Materials science of thin films: deposition and structure*. Academic press, San Diego
36. Assuncao V, Fortunato E, Marques A, Aguas H, Ferreira I, Costa MEV, Martins R (2003) *Thin Solid Films* 427:402
37. Gou L, Ran CQJ, Zheng C (1999) *Thin Solid Films* 345:42
38. Mikami Y, Yamada K, Ohnari A, Degawa T, Migita T, Tanaka T, Kawabata K, Kajioaka H (2000) *Surf Coat Technol* 133–134:295
39. Kuwahara K, Fujiyama H (1994) *IEEE Trans Plasma Sci* 22(4):442
40. Chan KY, Teo BS (2005) *J Mater Sci* 40:5971. doi: [10.1007/s10853-005-1362-8](https://doi.org/10.1007/s10853-005-1362-8)
41. Paul A, Wingbermühle J (2006) *J Appl Surf Sci* 252:8151
42. Wu ML, Kiely JD, Klemmer T, Hsia YT, Howard K (2004) *Thin Solid Films* 449:120
43. Musil J, Matous J, Vlcek J, Koydl L, Muller K (1994) *Czech J Phys* 44:565
44. Igasaki Y, Kanma H (2001) *Appl Surf Sci* 169–170:508
45. Cheng H, Sun Y, Hing P (2003) *Thin Solid Films* 434:112
46. Chawla V, Jayaganthan R, Chawla AK, Chandra R (2008) *Mater Chem Phys* 111:414
47. Mitra R, Hoffman RA, Madan A, Weertman JR (2001) *J Mater Res* 16:1010
48. Shinmitsu T, Shi J, Hashimoto M (2002) *Surf Coat Technol* 151:55
49. Almtoft KP, Bottiger J, Chevallier J, Schell N, Martins RMS (2005) *J Mater Res* 20:1071
50. Chan KY, Teo BS (2007) *Microelectron J* 38:60
51. Thornton JA (1986) *J Vac Sci Technol A* 4:3059
52. Thornton JA (1974) *J Vac Sci Technol* 11:666
53. Thornton JA (1975) *J Vac Sci Technol* 12:830
54. Qiu H, Nakai H, Hashimoto M, Safran G, Adamik M, Barna P, Yagi E (1994) *J Vac Sci Technol A* 12:2855
55. Ishino M, Yang J, Makihara K, Shi J, Hashimoto M (2000) *J Vac Sci Technol A* 18:2339
56. Shi J, Kojima D, Hashimoto M (2000) *J Appl Phys* 88:1679